MATERIALS PHYSICS AND MECHANICS REVIEW

Submitted: July 10, 2023 Revised: October 6, 2023 Accepted: December 25, 2023

Optimizing processing parameters for semi-solid casting: a comprehensive review

D.P. Singh [1]✉, V.K. Dwivedi [1], M. Agarwal [2],

[1] GLA University, Mathura, India

[2] Dr. Ram Manohar Lohia Avadh University, Faizabad, India

✉ devendraps.research@gmail.com

ABSTRACT

Semi-solid processing has gained popularity in the casting industry due to its significant advantages, offering a net shape single or multistep flexible process. This study aims to establish an evaluation criterion to understand the relationship between processability and its impact on outcomes. Pouring temperature and fluidity emerge as primary factors, while solidification and viscosity demonstrate secondary importance in the processing. Through a multi-angle evaluatory approach, the flexibility of all semi-solid casting process parameters can be assessed based on alloying elements, temperature gradient, fluidity, heat transfer, and solidification.

KEYWORDS

semi-solid casting • pouring temperature • solidification • temperature gradient • MMC

Citation: Singh DP, Dwivedi VK, Agarwal M. Optimizing processing parameters for semi-solid casting: a comprehensive review. *Materials Physics and Mechanics*. 2024;52(2): 1–10.
http://dx.doi.org/10.18149/MPM.5222024_1

Introduction

Semi-solid metal (SSM) processing is highly regarded as an attractive technique for manufacturing near-net-shape components with improved mechanical properties compared to traditional methods [1]. The concept of SSM processing emerged in the early 1970s, but its full understanding was achieved in later years, particularly after the 1990s. Initially, the understanding of SSM processing was limited, but it has now been linked to key processing parameters such as deformation rate, material fluidity, rheology (pseudo-plasticity and thixotropy), and pouring temperature [2]. Among these factors, fluidity, commonly expressed as fluidity length (L_f), plays a crucial role. L_f is defined as the distance covered by molten metal during forced flow in a small cross-section until solidification. It significantly influences the suggested solidification microstructures, which depend on the cooling rate [3,4]. Furthermore, during the semi-solid stage of liquid metallurgy, several other processing parameters come into play, including stirring action, squeeze pressure, pouring temperature, and pressurized solidification [5–11]. A semi-solid state is characterized by a higher fraction of solid than liquid within the melt, while a mushy state occurs just above the solidus line, where liquid metal is present during cooling. The liquid fraction is higher than the solid fraction in the semi-solid state. In both states, the behavior of the slurry resembles a thick (low viscous) material, depending on the presence of solidified grains within the melt [12]. The solid fraction affects the viscosity of the slurry, which is considered a suspension with dispersed solid particles exhibiting unique rheological properties such as pseudo-plasticity and thixotropy [13–28]. The melt temperature in liquid metallurgy plays a crucial role in determining the formation of states

Publisher: Peter the Great St. Petersburg Polytechnic University

such as semi-solid and mushy, which are determined by the solidus line of the parent material [29–31]. Intensive research has focused on the effects of semi-solid liquid metallurgy, as it offers improved properties with secondary parameters to control the pouring temperature of the melt. Figure 1 provides a summary of the organization of processing parameters and their effects. It has been identified that: fluidity and pouring temperature are vital processing parameters for controlling the solidification rate of the melt, inhibiting grain growth, promoting incomplete re-crystallization, and resulting in the formation of micro-fine grains.

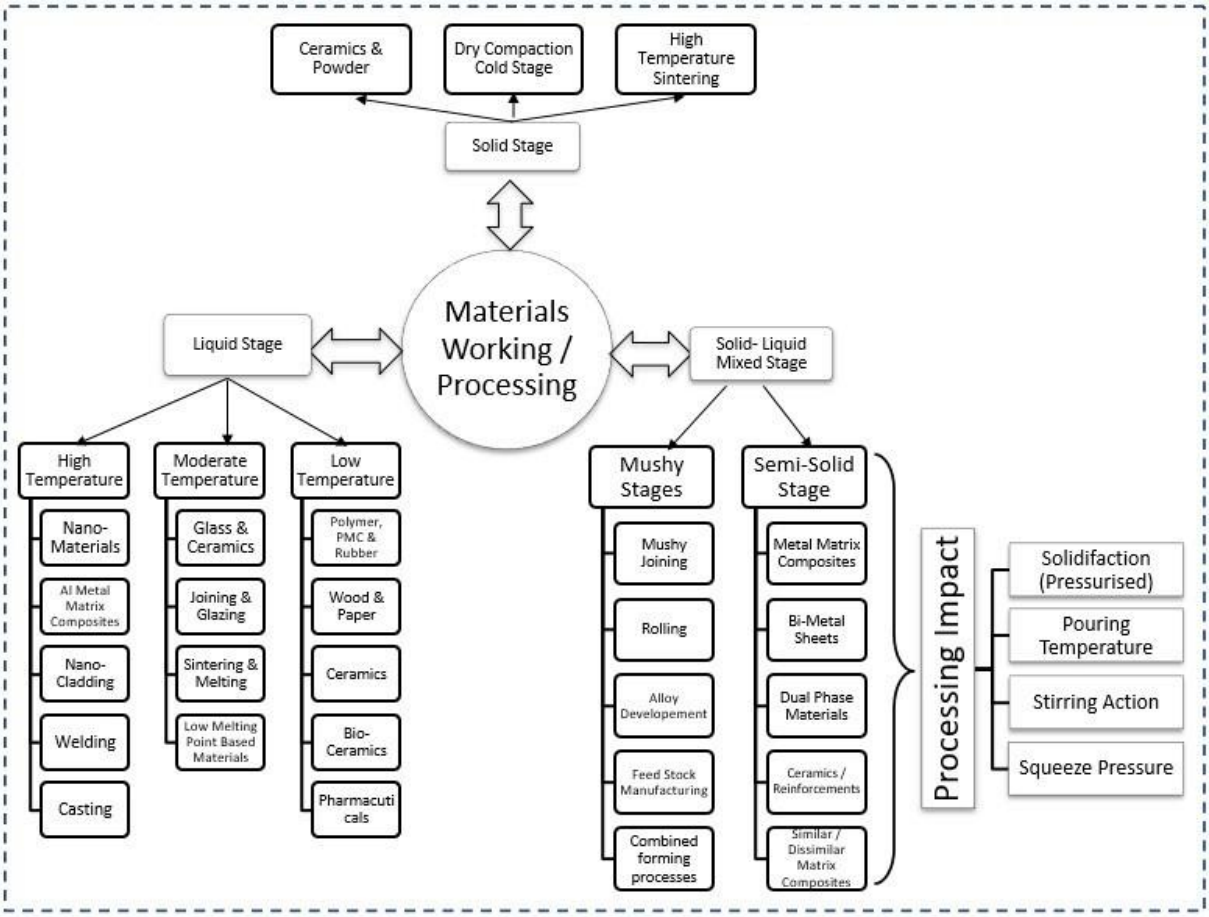

Fig. 1. Development of mushy/semi-solid material processing, parameters and application areas

These parameters can be controlled with the assistance of various associated parameters such as stirring action, reinforcement type, and squeeze pressure. However, this paper specifically discusses the effects of fluidity and pouring temperature on cast material properties and microstructure.

Impact of reinforcement on the fluidity and temperature

In the semi-solid casting process, a major challenge often encountered is achieving a high flow rate of semi-solid paste through thin sections and complex geometries [14]. Therefore, fluidity, which refers to the ability of the liquid metal to fill a mold, becomes a critical process parameter. Several factors contribute to fluidity determination, including molten metal characteristics such as viscosity, surface tension, suspended inclusions, mold design and material, pouring rate, superheat, and metal composition

[24–62]. Fluidity is inversely proportional to viscosity, viscosity index (sensitivity of viscosity to temperature), and freezing range. As these factors increase, fluidity decreases. Pure metals and eutectics with shorter freezing ranges exhibit higher fluidity, while alloys with longer freezing ranges tend to have lower fluidity [19,48]. The presence of high surface tension and oxide films on the liquid metal also reduces fluidity. Additionally, the inclusion of insoluble particles significantly affects fluidity, as they increase viscosity [20,51]. The dimensions of the runner, riser, and sprue in the mold also influence fluidity. Higher surface roughness of the mold and higher thermal conductivity of the mold material tend to decrease fluidity. Moreover, a slow pouring rate leads to reduced fluidity due to a higher cooling rate during slow pouring [21,40]. However, the most influential parameters governing fluidity are superheating, as higher temperature in the metal promotes greater flow in the mold, and metal composition, which impacts the mechanical and physical properties of the molten metal based on different alloying elements and their weight percentages [15–17,34–43].

Table 1. Effect of various alloying elements in Al-Base alloy

S. No.	Alloy	Alloying element	Effect of alloying on fluidity and temperature
1	A357	Copper	In the solid state the solubility of Cu in Al increases from less than 0.50 % at room temperature to 5.65 % at 821 K. Fluidity decreases along with ductility but also results better mechanical properties (hardness & strength) as Cu content increases. Thus, to have optimum ductility limited % of Cu (2 to 5 %) is beneficial and do not exceed 12 % in most Al-Cu based alloys [22].
2	Al-6Ni-3Si	Silicon	As an alloying element Si is used up to 14 % in amount. The solubility in Al, the α phase of Si is limited up to 1.65 % at 851 K and less than 0.05 % at room temperature. Up to eutectic % of Si, strength of Al-Si alloy increased by increasing Si% while ductility decreases. Like Mn and Ni, Si also do not confer response to solution heat treatment [23].
3	AZ91D and Mg–3Nd–0.2Zn–Zr	Magnesium	Magnesium behaves similar to copper when alloyed with aluminium. Solid-solubility change of the α phase with temperature reflects in alloy system. Solubility of Mg at 724 K is 14.9 % while at room temperature it is less than 2.90 %. If the solid-solubility limit is exceeded, A second, harder β phase exists. Aging and solution heat treatment can be done on this binary system which normally contain 4, 8, and 10 % of magnesium [24].
4	AlSi9Mg	Magnesium - Silicon	Some important alloying effects are reflected in aluminium by combination of Mg-Si which form the metallic compound Mg_2Si and produce a quasi-binary alloy system. Due to excess of Silicon present in Ternary alloys results improved casting properties like enhanced fluidity [25].
5	A357	Zinc	One of the principal alloying elements with major advantage that it makes possible to get maximum mechanical properties in the as-cast conditions but when it exceeds 0.1 to 0.3 %, it reduces corrosion resistance properties of alloy [22].
6	A356/TiB_2 + RE + Sn	Iron (as impurity)	Iron as impurity, omnipresent in amount of 0.8 to 2 % because iron can dissolve from ladles or from furnace pots and form Fe-Al phase which results embrittlement, reduced corrosion resistance ability & coarsening of as-cast grain size of metal [26].

Aluminum-based alloys, for example, are eutectic systems with various intermetallic compounds. Due to the lower solubility of most alloying elements in aluminum, these alloys exhibit multiple metallic phases with complex compositions [14,41]. Table 1 provides an overview of the effect of some key alloying elements such as Cu, Si, Mg, Zn, Cr, Mn, Sn, and Ti in aluminum-based casting alloys on fluidity and temperature.

Solidification and mechanism

After pouring, the solidification behavior of semi-solid slurry differs from conventional casting in the following aspects: the temperature gradient of the surrounding environment, the presence of constituent or alloying elements in the slurry, the mode of heat transfer [10,51].

These three conditions give rise to a solidification range, known as the freezing range, which is determined by the solidus and liquidus temperatures. Within this range, both primary and secondary solidification occur. Primary solidification initiates just before the liquidus temperature, while secondary solidification takes place over time. Figures 2 and 3 illustrate the time-dependent temperature curves.

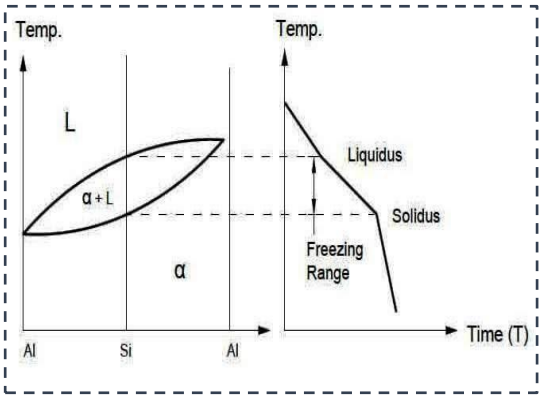

Fig. 2. Variations in temperature vs time for semi solid processing

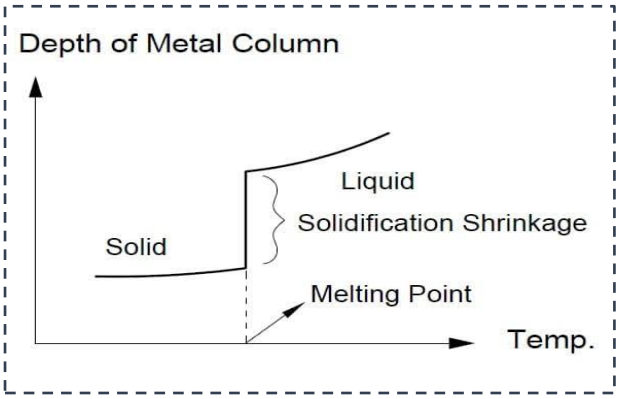

Fig. 3. Variations in depth of metal column vs temperature for semi solid processing

Above the liquidus temperature, the fluidity of the slurry is influenced by gravitational and convection effects and is affected by the thermal conductivity of the mold. In this temperature range, the primary solidification range is narrower compared to the secondary solidification range. This phenomenon, known as liquid solidification shrinkage (Fig. 4), is influenced by the presence of unmelted solid particles, such as reinforcement ceramics, hindering the movement of silicon particulates in the α-Al melt. A thermal mismatch between the solid particles and the liquid melt enhances the temperature gradient, leading to a decrease in solidification time. Gravitational and convection effects contribute to the formation of columnar grains and equiaxed grains during the tertiary solidification zone, which is primarily observed in liquid-liquid solidification. The formation of these grains is influenced by factors such as the depth of the metal column, temperature gradient, and available solidification time [10]. Local solidification, governed by the secondary solidification zone (Fig. 5), is also affected. The

total solidification time depends on the pouring temperature of the melt, which is governed by the α-cooling rate [10,40–42]. Figure 5 illustrates the "semi-solid pouring zone" (AB) as part of the total solidification time. In the actual solidification time, local solidification is influenced by alloying particulates/elements, leading to a decrease in the secondary solidification range and an increase in the primary solidification range due to a higher thermal gradient (A'B'). However, the total solidification time is less hindered in conventional slurry melts, where the time zone mostly increases for tertiary solidification (CD C'D', Fig. 5). This is referred to as the "thermal arrest zone", where sensible heat transfer is higher compared to latent heat transfer, resulting in a difference between secondary solidification and tertiary solidification. Figure 4 represents the effect of fluidity, showing the solidification starting range, phase transition range, and secondary solidification range. The solidification process after the phase transition, up to the solidification temperature, involves latent heat transfer and takes more time compared to primary and tertiary solidification [10,62].

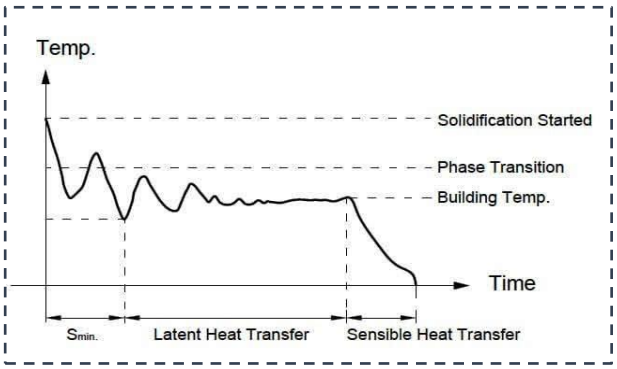

Fig. 4. Variations showing for temperature and time for heat transfer and phase transformation

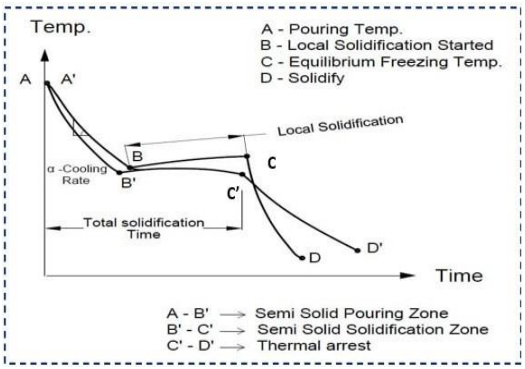

Fig. 5. Variations showing for temperature and time for effect of pouring temperature and solidification

Thermodynamic- equilibrium, interface and solidification

Thermodynamics plays a crucial role in analyzing the solidification phase composition and the resulting interfacial effects [6,10,39]. The slopes of liquidus variations, solidus phase boundaries, and solidification paths are correlated with the constituent temperature of the melt during solidification. The degree of undercooling, which is related to the type of matrix and reinforcement, directly impacts interface formation. Different types of interfaces can be formed, including: local interface equilibrium, interface non-equilibrium, equilibrium departure, and pressurized undercooling.

These interfaces are influenced by the solidus and liquidus phenomena of the pouring temperature, with Gibbs' free energy directly linked to the formation of interfaces at various stages. The correlation between solidification and interfaces can be determined by examining the steps involved in the solidification process.

Well known Gibb's free energy:

$$G = H - T.S \quad (1)$$

where $H = E + Pv$ (enthalpy of phase neutral alloy).

Considering three steps of the semi-solid melt before solidification:
(1) Liquidus stage (G_1);
(2) Liquidus/Solidus stage (liquid in majority) (G_2);
(3) Solidus/Liquidus stage (solid in majority) (G_3).

Difference of Gibb's free energy from initial to final stage:

$$\Delta G = (G_1 - G_2) + G_2' - G_3 \quad , \tag{2}$$

where G_2'- the Gibb's free energy due to the impact of reinforcement. Generally,

$$G_2' > G_2 - \Delta G_2 = G_l - G_s. \tag{3}$$

However, $G_2 > \Delta G_2 > G_2'$:

$$\Delta G_2 = (H_l - H_s) - T_e(S_l - S_s) = 0 \text{ (for pure metal)}, \tag{4}$$

$$\Delta G_2 = (H_l - H_s) - T_e(S_l - S_s) \neq 0 \text{ (for reinforced metal)}. \tag{5}$$

Further,

$$\Delta H = (\Delta S_f) T_e \tag{6}$$

where, ΔH is change in enthalpy during the melting, ΔS_f entropy of the fused solidus particle, T_e is equivalent temperature (mean value).

Now, as T_e decreases:

$$\Delta G_2 = \Delta H_f \left(\frac{T_e - T'}{T_e}\right), \tag{7}$$

where $T'$is temperature at a particular stage. As T' decreases solidification increases:

$$\Delta G_2 = \Delta H_f \left(\frac{\Delta T'}{T_e}\right) \tag{8}$$

$$\Delta G_2 = \Delta S_f \Delta T', \tag{9}$$

where $\Delta T'$is considered for undercooling.

According to the above equations, liquid in majority is considered for the liquidus stage for Gibb's free energy G_2 used in the above equations. Further, this stage is variable and changes appears due to the type and amount of reinforcement incorporation for which Gibb's free energy is much higher as compare to the unmodified liquid conditions as shown in Eq. (3). Generally, change in Gibb's free energy due to the incorporation of reinforcement is increases in initial stage, whereas this can be considerable as 'zero' for the pure metal and ideal condition as shown in Eqs. (4) and (5).

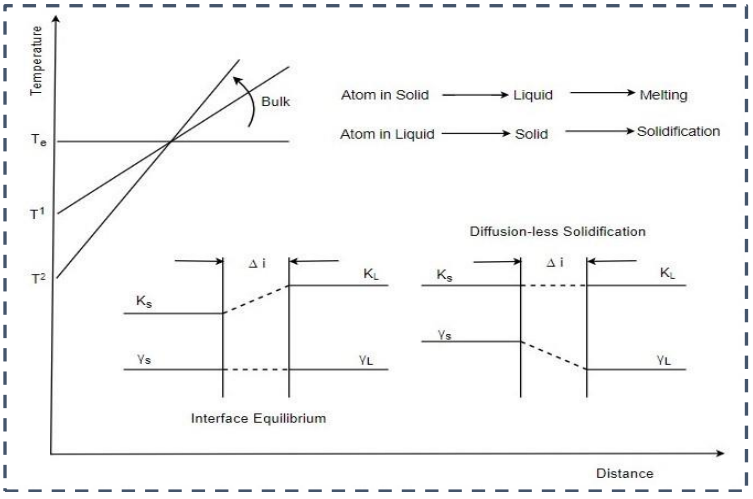

Fig. 6. Relation between temperature and distance for Interfacial and diffusion-less solidification

Equations (6-9) and (10) show the correlation between enthalpy and entropy with the equilibrium temperature, as shown in Fig. 6. Here, according to Fig. 6 and Eqs. (6-9) and (10), change in enthalpy and entropy for the fused solid particles is a potential candidate and parameter for the equilibrium temperature under pressurized solidification [59]. Generally, equilibrium temperature is a function of a particular stage (T) in which solidification started. T is dependent on the type of reinforcement and its incorporation, while ΔH_f is the change in enthalpy for the liquid melt. As the amount of reinforcement increases T decreases solidification rate increases which is an obvious phenomenon [7,24,40,51]. This shows the condition of undercooling according to Eq. (10) while as under undercooling condition, ΔT becomes positive and solidification rate is considered as a function of enthalpy and entropy. Moreover, for no undercooling condition:

$\Delta T = 0$ however $\Delta G = 0$. (10)

System is in equilibrium and no transformation is existed. This is the general and possible condition of self-pouring temperature under gravity of melt.

Free energy under pressurized cooling $\Delta F_{l|_s} = \Delta F_l - \Delta F_s$

$$\Delta F_l = \Delta P(v_l - v_s) - \Delta T(S_l - S_s) \quad (11)$$

The change in equilibrium temperature due to applied pressure:

$$\Delta T = \frac{\Delta v}{\Delta S_f}\Delta P. \quad (12)$$

This pressure is the function of temperature. As the temperature of the slurry decreases, pressurized solidification increases. As $\Delta P > 0$ result is increase in undercooling. This is converted to kinetic undercooling for solid to liquid interface. Generally, solidification velocity depends on the rate of solidification and rate of melting [10,62]. However,

$$v = v_s - v_s e^{\left(\frac{\Delta G}{RT_i}\right)}, \quad (13)$$

where ΔG is in J/mole and $\boldsymbol{v_s}$ is the hypothetical maximum growth of the velocity.

Table 2. Effect of the increment in undercooling or solidification

Diffusional equilibrium	**Interfacial equilibrium**	**Interfacial non-equilibrium**
Absence of temperature gradient	Liquid-solid interface for temperature	Arbitrary impact of temperature gradient
Uniform phase composition	Metastable phase condition	Phase diagram fails to evaluate the compositions on local interface zone

Equations (11-13) describe the thermodynamic equilibrium conditions for undercooling and interfacial stages, involving ΔG (change in Gibbs free energy) and the growth velocity of solidification [10]. Equation (11) represents pressurized solidification, where interface equilibrium occurs when the thermal conductivity of the reinforcement is the dominant factor [39,46,59]. At this stage, interface formation increases, and interface equilibrium is sustained, as depicted in Fig. 6 and described by Eqs. (11), (12). After a certain point, incomplete recrystallization occurs due to these interfaces, and diffusion solidification begins [10,60]. Diffusion solidification leads to the transformation of micro level reinforcement particles near the interface boundaries, causing an increase in the growth of solid particles. As a result, there is a drop in solidification velocity, as shown in Fig. 6. In the semi-solid stage, the temperature conditions T1 and T2 represent

the solid and liquid candidates present in the slurry, respectively. These conditions give rise to several thermally dependent stages, including: constitutional undercooling, Conditional and unconditional undercooling, and interfacial thermal undercooling.

Undercooling plays a dominant role in the solidification process in the semi-solid stage and contributes to the formation of different thermal interfaces and undercooling conditions, as summarized in Table 2.

Conclusions

This review primarily focuses on the research findings related to semi-solid casting, specifically exploring the impact of processing temperature, alloying elements, and fluidity as crucial parameters. The solidification rate, considered a secondary parameter, is also influenced by factors such as pouring temperature, holding time, and stirring action, which are essential for controlling the slurry. Moreover, restricted grain growth plays a significant role in the solidification behavior, influenced by the solid-liquid fraction and viscosity of the slurry. This correlation between rheological properties and processing parameters establishes the cohesion within the system. Additionally, the temperature gradient, as an associated processing parameter, affects the heat transfer mode during solidification and is influenced by the alloying elements, resulting in different types of solidification shrinkage. In summary, all the selected criteria are interconnected, playing a crucial role in the overall processing, phase transition, and solidification processes.

References

1. Kirkwood DH. Semi-solid metal processing. *International Materials Reviews*. 1994;39(5): 173–189.
2. Fan Z. Semi-solid metal processing. *International Materials Review*. 2002;47: 249–285.
3. Morando C, Fornaro O, Garbellini O, Palacio H. Fluidity on metallic eutectic alloys. *Procedia Materals Science*. 2015;8: 959–967.
4. Alrobei H. Effect of different parameters and aging time on wear resistance and hardness of SiC-B4C reinforced AA6061 alloy. *Journal of Mechanical Science and Technology*. 2020;34: 2027–2034.
5. Singh DP, Dwivedi VK, Agarwal M. The key attributes of processing parameters on semi-solid metal casting: An Overview. *E3S Web of Conferences*. 2021;309: 01089.
6. Miazga A, Konopka K, Gizowska M, Szafran M. Alumina matrix ceramic-nickel composites formed by gel-casting method. *Composites Theory and Practice*. 2012;12(2): 138–141.
7. Agarwal M, Srivastava R. Influence of processing parameters on microstructure and mechanical response of a high-pressure die cast aluminum alloy. *Materials and Manufacturing Processes*. 2019;34(4): 462–472.
8. Agarwal M, Srivastava R. Influence of fine Al2O3 and aluminium nano-particles on the 6061 aluminium alloy near the grain boundary of the semisolid cast microstructure. *Transactions of the Indian Ceramic Society*. 2019;78(2): 94–100.
9. Agarwal M, Srivastava R. Effect of thick slurry and stepped deformation on mechanical properties of AA6061 alloys. *Emerging Materials Research*. 2019;8(3): 394-403.
10. Agarwal M, Dixit NK, Dixit M, Srivastava R. Interfacial study for the effect of Al2O3 addition on the microstructure and micro-hardness of the Al2O3/AA6061 semi-solid cast composite. *Phase Transitions*. 2021;94(12): 899–909.
11. Chen S, Chang G, Yue X, Li Q. Solidification process and microstructure of transition layer of Cu–Al composite cast prepared by method of pouring molten aluminum. *Transactions of Nonferrous Metals Society of China*. 2016;26(8): 2247–256.
12. Deev VB, Ponomareva KV, Kutsenko AI, Prikhodko OG, Smetanyuk SV. Influence of temperatures of melt overheating and pouring on the quality of aluminum alloy lost foam castings. *Russian Journal of Non-Ferrous Metals*. 2017;58: 373–377. (In Russian)
13. Sui Y, Feng K, Cheng C, Chen X, Qi J, He Y, Meng Q, Wei F, Sun Z. Effects of pouring temperature on interfacial reaction between Ti-47.5Al-2.5V-1Cr alloy and mold during centrifugal casting. *Journal of Wuhan University of Technology-Mater. Sci. Ed.* 2016;31: 1105–1108.
14. Heo M, Jin CK, Roh JS, Kang CG. Investigating the micro-structures of A356 semi-solids based on electromagnetic stirring currents and crucible materials. *Journal of Mechanical Science and Technology*. 2020;34: 3807–3813.

15. Kim JH, Yasukawa A, Yonezawa S. Enhanced dispersion stability and fluidity of rutile TiO_2 particles using surface fluorination. *Materials Today: Proceedings*. 2020;20: 311–319.
16. Sang-Su N, Yong-Ho K, Hyeon-Taek S, Seong-Hee L. Effect of Sc addition on microstructure, electrical conductivity, thermal conductivity and mechanical properties of Al-2Zn-1Cu-0.3Mg based Alloy. *Korean Journal of Materials Research*. 2020;30(10): 542–549.
17. Mishra RR, Sharma AK. Microwave heating characteristics of bulk metallic materials and role of oxides. *Journal of Materials Science*. 2018;53: 16567–16584.
18. Olszówka-Myalska A, Myalski J, Wrzała K. Fabrication of magnesium matrix composite with glassy carbon particles by pressure die casting. *Composites Theory and Practice*. 2014;14(2): 101–105.
19. Motoyama Y, Tokunaga H, Yoshida M, Maruyama T, Okane T. Measuring the interfacial heat transfer coefficient between flowing molten alloy and sand mold using fluidity tests. *Journal of Materials Processing Technology*. 2019;11: 6394.
20. Fu Y, Wang H, Zhang C, Hao H. Effects of minor Sr additions on the as-cast microstructure, fluidity and mechanical properties of Mg-4.2Zn-1.7RE-0.8Zr-0.2Ca (wt%) alloy. *Materials Science and Engineering: A*. 2018;723: 118–125.
21. Birru AK, Kumar BP. Influence of fluidity of Al-Cu alloy with fly ash reinforcement by single spiral fluidity test. *Materials Today: Proceedings*. 2015;24(5): 2776–2783.
22. Mao G, Liu D, Gao W, Liu S, Zhong L. The effects of copper (Cu) or zinc (Zn) on fluidity of A357 alloy. *Materials Letters*. 2021;304: 130733.
23. Yang L, Li W, Du J, Wang K, Tang P. Effect of Si and Ni contents on the fluidity of Al-Ni-Si alloys evaluated by using thermal analysis. *Thermochimica Acta*. 2016;6: 457–415.
24. Huang H, Wang YX, Fu PH, Peng LM, Jiang HY, Xu WY. Fluidity of AZ91D and Mg–3Nd–0·2Zn–Zr (wt-%) magnesium alloys: response to pouring and mould temperature. *International Journal of Cast Metals Research*. 2013;26(4): 213–219.
25. Qi Z, Miao C, Jin C. AlSi9Mg aluminum alloy semi-solid slurry preparation by intermediate frequency electromagnetic oscillation process. *Journal of Materials Processing Technology*. 2015;215: 42–49.
26. Rathod N, Menghani J. Detrimental effect of Fe as impurity on A356/TiB2 + RE + Sn alloy fabricate via in situ route. *Materials Today: Proceedings*. 2021;44(1): 1326–1330.
27. Ragab KA, Bouaicha A, Bouazara M. Optimization of casting design parameters on fabrication of reliable semi-solid aluminum suspension control arm. *Journal of Materials Engineering and Performance*. 2017;26: 4450–4461.
28. Liu Z, Mao W, Wang W, et al. Investigation of rheo-diecasting mold filling of semi-solid A380 aluminum alloy slurry. *International Journal of Minerals, Metallurgy and Materials*. 2017;24: 691–700.
29. Srivastava A, Shaikh KA, Bopanna S. Microstructural Characterization of SiC reinforced Ti–6Al–4V metal matrix composites fabricated through powder metallurgy route. *Materials Physics and Mechanics*. 2023;51(3): 29–37.
30. Zemtsova EG, Smirnov VM, Kozlova LA, Morozov PE, Yurchuk DV, Semenov BN, Morozov NF. Development of aluminum-based composite with two reinforcing modifiers (TiC/Ni, CNTs/Ni) with improved mechanical properties. *Materials Physics and Mechanics*. 2023;51(3): 9–19.
31. Ravikumar M, Naik R, Vinod BR, Chethana KY, Rammohan YS. Study on nanosized Al2O3 and Al2O3-SiC on mechanical, wear and fracture surface of Al7075 composites for soil anchoring applications. *Materials Physics and Mechanics*. 2023;51(6): 24–41.
32. Prasad KS, Mukhopadhyay AK, Majumdar B, Akhtar D. Nature and stability of phases present in a rapidly solidified aluminium alloy 7010 containing scandium. *Materials and Manufacturing Processes*. 2008;23(7): 658–664.
33. Ragab KA, Bouazara M, Bouaicha A, Allaoui O. Microstructural and mechanical features of aluminium semi-solid alloys made by rheocasting technique. *Materials Science and Technology*. 2017;33(6): 646–655.
34. Kolahdooz A, Aminian S. Effects of important parameters in the production of Al-A356 alloy by semi-solid forming process. *Journal of Materials Research and Technology*. 2019;8(1): 189–198.
35. Ansari MHS, Aghaie-Khafri M. Predicting flow localization in semi-solid deformation. *International Journal of Material Forming*. 2018;11: 165–173.
36. Simlandi S, Barman N, Chattopadhyay H. Study on rheological behavior of semisolid A356 alloy during solidification. *Transactions of the Indian Institute of Metals*. 2012;65: 809–814.
37. Nikanorov SP, Osipov VN, Regel LI. Structural and mechanical properties of directionally solidified Al-Si alloys. *Journal of Materials Engineering and Performance*. 2019;28: 7302–7323.
38. Li M, Li Y, Bi G, Huang X, Chen T, Ma Y. Effects of melt treatment temperature and isothermal holding parameter on water-quenched microstructures of A356 aluminum alloy semisolid slurry. *Transactions of Nonferrous Metals Society of China*. 2018;28(3): 393–403.
39. Pang S, Wu G, Liu W, Zhang L, Zhang Y, Conrad H, Ding W. Influence of pouring temperature on solidification behavior, microstructure and mechanical properties of sand-cast Mg-10Gd-3Y-0.4Zr alloy. *Transactions of Nonferrous Metals Society of China*. 2015;25(2): 363–374.
40. Birol Y. A357 thixoforming feedstock produced by cooling slope casting. *Journal of Materials Processing Technology*. 2007;186(1-3): 94–101.
41. Alhejazi HJ, Maijer DM, Macht JP, Phillion AB. Comparison of semi-solid contraction of aluminum alloys during solidification quantified by a combined numerical-experimental approach. *Metals and Materials International*. 2022;28: 1783–1793.

42. Birol Y. Semi-solid processing of the primary aluminium die casting alloy A365. *Journal of Alloys and Compounds*. 2009;473(1-2): 133–138.
43. Pulivarti SR, Birru AK. Effect of mould coatings and pouring temperature on the fluidity of different thin cross-sections of A206 Alloy by sand casting. *Transactions of the Indian Institute of Metals*. 2018;71: 1735–1745.
44. Zou GT, Zhang HH, Yang YT, Lu FM, Yu ZT, Wang C. Effects of pouring and mold temperatures on the fluidity and hot tearing susceptibility of Al–3.5Si–0.5Mg–0.4Cu alloy. *Transactions of the Indian Institute of Metals*. 2020;73: 2511–2517.
45. Shehata MM, El-Hadad S, Moussa ME, El-Shennawy M. Optimizing the pouring temperature for semisolid casting of a hypereutectic Al–Si alloy using the cooling slope plate method. *Inter Metalcast*. 2021;15: 488–499.
46. Liu G, Wang Q, Zhang L, Ye B, Jiang H, Ding W. Effects of melt-to-solid volume ratio and pouring temperature on microstructures and mechanical properties of Cu/Al bimetals in compound casting process. *Metall Mater Trans A*. 2019;50: 401–414.
47. Fehlbier M, Klaassen O, Salun PR. Semi-solid-metal casting/thixocasting: determination of the flow characteristics of semi-solid aluminium alloys. In: Winkler PJ. (ed.) *Materials for Transportation Technology*. Weinheim, Germany: Wiley-VCH Verlag GmbH; 2000. p.124–128.
48. Balitchev E, Hallstedt B, Neuschütz D. Thermodynamic criteria for the selection of alloys suitable for semi-solid processing. *Steel Research International*. 2005;76(2-3): 92–98.
49. Li L, Li D, Feng J, Zhang Y, Kang Y. Effect of cooling rates on the microstructure and mechanical property of La modified Al7SiMg alloys processed by gravity die casting and semi-solid die casting. *Metals*. 2020;10(4): 549.
50. Talangkun S, Potisawang C, Saenpong P. Thixoforming and rheo-die-casting of A356/SiC composite. *Metals*. 2020;10(2): 251.
51. Stefanescu DM. Equilibrium and non-equilibrium during solidification. In: *Science and Engineering of Casting Solidification*. Second Edition. Boston, MA: Springer; 2009. p.1–20.
52. Cao Fx, Deng KK, Wang CJ, Nie K, Liang W, Fan J. Synergistic enhancement of the strength-ductility for stir casting SiCp/2024 Al composites by two-step deformation. *Metals and Materials International*. 2021;27: 5450–5461.
53. Samavedam S, Sakri SB, Hanumantha RD, Sundarrajan S. Estimation of porosity and shrinkage in a cast eutectic Al–Si alloy. *Canadian Metallurgical Quarterly*. 2014; 53(1): 55–64.
54. Birol Y. Cooling slope casting and thixoforming of hypereutectic A390 alloy. *Journal of Materials Processing Technology*. 2008;207(1-3): 200–203.
55. Aguilar J, Fehlbier M, Grimmig T, Bramann H, Afrath C, Bührig AP. Semi-solid processing of metal alloys. *Steel Research International*. 2004;75: 492–505.
56. Mishra RR, Sharma AK. Microwave–material interaction phenomena: heating mechanisms, challenges and opportunities in material processing. *Composites Part A: Applied Science and Manufacturing*. 2016;81: 78–97.
57. Han J, Liu Z, Jia Y, Wang T, Zhao L, Guo J, Chen Y. Effect of TiB2 addition on microstructure and fluidity of cast Ti-Al alloy. *Vacuum*. 2020;174: 109210.
58. Mao J, Liu W, Wu G, et al. Semi-solid slurry preparation, rheo-die casting and rheo-squeeze casting of an AZ91–2Ca–1.5Ce ignition-proof magnesium alloy by gas-bubbling process. *Journal of Materials Research*. 2017;32: 677–686.
59. Moustafa SF. Casting of particulate Al-base composites. *International Journal of Materials Research*. 1997;88(3): 209–216.
60. Tuan NA, Van LD, Giang LD. Optimization of Processing Parameters of Primary Phase Particle Size of Cooling Slope Process for Semi-solid Casting of ADC 12 Al Alloy. In: Bui TQ, Cuong LT, Khatir S. (eds.) *Structural Health Monitoring and Engineering Structures. Lecture Notes in Civil Engineering*. Singapore: Springer; 2021. p.49–61.
61. Midson SP. Using micro-CT scanning to quantitative characterizes porosity in high pressure die castings and semi-solid castings. *In: Solid State Phenomena*. 2022;327: 33–44.
62. Yumi K, Youngchan K, Seweon C. Effect of precipitation and dissolution of Si on the thermal diffusivity in the Al-Si alloy system. *Korean Journal of Materials Research*. 2020;30(9): 474–479.

About Authors

Devendra Pratap Singh
Research Scholar, GLA University, Mathura, India

Dwivedi Vijay Kumar
Professor, GLA University, Mathura, India

Mayank Agarwal
PhD, Associate Professor, Dr. RML Avadh University, Faizabad, India